Multiplicity dependence of χ_c and χ_b meson production

Marat Siddikov and Iván Schmidt
Departamento de Física, Universidad Técnica Federico Santa María,
y Centro Científico—Tecnológico de Valparaíso, Casilla 110-V, Valparaíso 2390123, Chile

(Received 17 December 2020; accepted 1 July 2021; published 23 July 2021)

We analyze in detail the production of χ_c and χ_b mesons in pp collisions. Using the color dipole framework, we estimate the cross sections in the kinematics of ongoing and forthcoming experiments and find that our estimates are in reasonable agreement with currently available experimental data. We also analyze the dependence on multiplicity of coproduced hadrons and find that it is significantly milder than that of S-wave quarkonia. We expect that an experimental confirmation of this result could constitute an important test of our understanding of multiplicity enhancement mechanisms in the production of different quarkonia states.

DOI: 10.1103/PhysRevD.104.016023

I. INTRODUCTION

Currently, the production of mesons containing heavy quarks can be described reasonably well in completely different approaches, like gluon-gluon or Pomeron-Pomeron fusion and the color dipole approach (see [1–4] for overviews). This success is largely attributable to the fact that in the heavy quark mass limit the partonic-level subprocess becomes essentially perturbative, thereby reducing the differences between the frameworks. Although all the frameworks provide reasonable phenomenological estimates, the parameters needed for the description of late-stage hadronization [like fragmentation functions of open-flavor D or B mesons or the long-distance matrix elements (LDMEs) of quarkonia states] might differ quite considerably [5–7], challenging their expected universality. Moreover, the approaches based on gluon-gluon (Pomeron-Pomeron) fusion recently encountered difficulties with the description of new experimental data on multiplicity dependence of coproduced charged hadrons [8–13]. In fact, it was discovered by both the STAR and ALICE collaborations that the relative yields of the $1S$ quarkonia grow vigorously as a function of multiplicity. This enhancement is seen in AA, pA [14,15], and even pp collisions [16,17], which clearly signals that it is not related to collective effects. Similar enhancement was observed for D meson and nonprompt J/ψ production [8]. As mentioned in [18], these new findings cannot easily be accommodated in the framework of models based on the two-Pomeron fusion picture and thus potentially could require the introduction of new mechanisms for both AA and pp collisions.

Since early studies of high energy production in the Regge approach [19–24], it has been established that multiplicity enhancement might be related to contributions of multiple Pomeron exchanges, and for this reason the approaches based on gluon-gluon or Pomeron-Pomeron fusion explain the observed multiplicity enhancement in J/ψ and D meson production [25–30] via contributions of additional multi-Pomeron states. It is expected that such contributions might be quite pronounced, and in the case of D meson production might be responsible for up to 40% of all the produced D mesons in inclusive production. This contribution is quite substantial and challenges the anticipated dominance of gluon-gluon (Pomeron-Pomeron) mechanism.

To better understand the microscopic mechanisms of multiplicity enhancement in heavy quarkonia production, it is very desirable to extend the currently available experimental data and study the multiplicity dependence in other channels. For example, we suggested [31] studying the multiplicity dependence in diffractive production, which has a slightly different underlying mechanism. However, the predicted cross section for this channel is much smaller than for the inclusive case due to certain process-specific factors, and for this reason its multiplicity dependence could be studied only during High Luminosity Run 3 at the LHC [32–34]. In this paper we explore another possibility and suggest studying the multiplicity dependence of coproduced hadrons in the production of P-wave quarkonia, e.g., the lightest χ_c and χ_b mesons. The production cross sections of these mesons are comparable by order of magnitude to the cross sections of J/ψ and $\Upsilon(1S)$, respectively, which should guarantee a reasonable statistics for high-multiplicity studies. The production of χ_c mesons has been extensively studied in the k_T factorization approach in [35–42], where it was found that a two-gluon ($\approx$ two-Pomeron) fusion mechanism provides a good description of the available data on its rapidity and transverse momentum dependence. Moreover, the color octet mechanism for P-wave quarkonia gives a small contribution due to the smallness of the LDMEs [35–37], so this fact minimizes the inherent uncertainty related to this mechanism. On the other hand, because of spin-orbital interactions, the P-wave quarkonia show up as a triplet of states with different angular momenta: $J = 0$, 1, or 2. Independent studies of production cross sections for each of these states provides a sensitive test of the underlying production mechanism. For this reason, we believe that P-wave quarkonia are ideally suited for the study of the multiplicity enhancement mechanisms. Since we are interested in the multiplicity dependence in the small-x kinematics, instead of k_T factorization we will use a color dipole framework (also known as CGC/Saturation or CGC/Sat) [43–51]. This framework allows one to systematically take into account contributions of multiple Balitsky-Fadin-Kuraev-Lipatov (BFKL) Pomeron states. The generalization of the color dipole approach to high-multiplicity events is well known in the literature [52–61].

The paper is structured as follows. In Sec. II we describe a framework for χ_{cJ} and χ_{bJ} quarkonia production. In Sec. III we make numerical estimates of the cross sections, compare them with the available experimental data, and make predictions for future experiments. In Sec. IV we evaluate the dependence on multiplicity. Finally, in Sec. V we draw some conclusions.

II. PRODUCTION MECHANISMS OF P-WAVE QUARKONIA

The high-energy inclusive production of heavy quarkonia might be considered a scattering of the projectile gluon on a proton via formation of a virtual heavy $\bar{Q}Q$ pair and the hadronization of the latter into quarkonium state M, as shown in Fig. 1. In the kinematics of LHC experiments, the average light-cone momentum fractions $x_{1,2}$ carried by gluons are very small ($\ll 1$) and the gluon densities are enhanced. This enhancement implies that there could be sizable corrections from multiple gluon exchanges between the heavy dipole and the target, which are formally suppressed in the heavy quark mass limit. For this reason, instead of a hard process on individual partons, it is more appropriate to use the CGC/Sat framework [43–51]. The color dipoles are eigenstates of interaction at high energies and, for this reason, can be used as universal elementary building blocks automatically accumulating both hard and soft fluctuations [62]. In fact, the light-cone color dipole framework has been successfully applied to phenomenological descriptions of both hadron-hadron and lepton-hadron collisions [63–70]. Another advantage of the CGC/Sat framework is that it allows a relatively straightforward extension for the description of high-multiplicity events, as discussed in [52–59]. The cross section of quarkonia production process, as shown in Appendix A, is given by

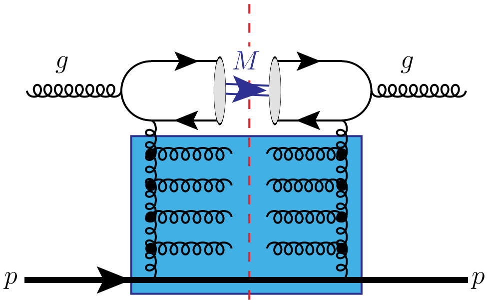

FIG. 1. Color dipole picture of the P-wave quarkonia hadroproduction in a gluon-proton collision. The colored squared block in the inferior part of the diagram contains all possible multigluon (multi-Pomeron) interactions which are included in the dipole amplitude. The vertical dashed line represents unitarity cuts. The produced meson M is shown with a double line and arrow.

$$\frac{d\sigma_M(y,\sqrt{s})}{dyd^2p_T} = \int d^2k_T x_1 g(x_1, \boldsymbol{p}_T - \boldsymbol{k}_T) \int_0^1 dz_1 \int_0^1 dz_2 \int \frac{d^2r_1}{4\pi} \int \frac{d^2r_2}{4\pi} \int d^2\boldsymbol{b}_{21} e^{i\boldsymbol{b}_{21}\cdot\boldsymbol{k}_T} \\ \times \langle \Psi^\dagger_{\bar{Q}Q}(r_1,z_1)\Psi_M(r_1,z_1)\rangle \langle \Psi^\dagger_{\bar{Q}Q}(r_2,z_2)\Psi_M(r_2,z_2)\rangle^* N_M(x_2; z_1, \boldsymbol{r}_1; z_2, \boldsymbol{r}_2; \boldsymbol{b}_{21}) + (x_1 \leftrightarrow x_2), \tag{1}$$

$$N_M(x; z_1, \boldsymbol{r}_1; z_2, \boldsymbol{r}_2; \boldsymbol{b}_{21}) = N(x, \boldsymbol{b}_{21} + \bar{z}_2\boldsymbol{r}_2 + \bar{z}_1\boldsymbol{r}_1) + N(x\boldsymbol{b}_{21} - z_1\boldsymbol{r}_1 - z_2\boldsymbol{r}_2) \\ - N(x, \boldsymbol{b}_{21} + \bar{z}_2\boldsymbol{r}_2 - z_1\boldsymbol{r}_1) - N(x, \boldsymbol{b}_{21} - \bar{z}_1\boldsymbol{r}_1 - z_2\boldsymbol{r}_2), \tag{2}$$

$$x_{1,2} \approx \frac{\sqrt{m_M^2 + \langle p_{\perp M}^2 \rangle}}{\sqrt{s}} e^{\pm y}, \tag{3}$$

where y and p_T are the rapidity and transverse momenta of the produced quarkonia in the center-of-mass frame of the colliding protons, $(z_i, \boldsymbol{r}_i)$ are the light-cone fractions of the quark and the transverse separation between quarks inside the dipole (with subindices $i = 1, 2$ representing the amplitude and its complex conjugate, respectively), and $\boldsymbol{b}_{21}$ is the difference of impact parameters of the dipoles in the amplitude and its conjugate. We also use the notation $\Psi_M(r, z)$ for the light-cone wave function of quarkonium M ($M = \chi_c, \chi_b$), and $\Psi_{\bar{Q}Q}$ for the quark-antiquark component of the gluon light-cone wave function (for the sake of completeness both are discussed in detail in Appendix B). The amplitude N_M depends on a linear combination of forward dipole scattering amplitudes $N(y, \boldsymbol{r}) \equiv \int d^2\boldsymbol{b} N(y, \boldsymbol{r}, \boldsymbol{b})$, as given in Eq. (2). This expression was derived in the heavy quark mass limit, when the typical dipole sizes are small. This smallness allows us to disregard additional quadrupole contributions which were studied in detail in [71]. The notation $x_g g(x_g, \boldsymbol{k}_T)$ in Eq. (1) is used for the unintegrated gluon parton distribution function (uPDF). The expression for the p_T-integrated cross section has a similar structure and differs only by the replacement of the gluon uPDF $x_1 g(x_1, \boldsymbol{p}_T - \boldsymbol{k}_T)$ with the integrated PDF $x_1 g(x_1, \mu_F)$, taken at the scale $\mu_F \approx 2m_Q$. The integrated gluon PDF $x_1 g(x_1, \mu_F)$ in the CGC/Sat approach is closely related to the dipole scattering amplitude $N(y, \boldsymbol{r})$ introduced earlier as [52,72]

$$\frac{C_F}{2\pi^2 \bar{\alpha}_S} N(y, \boldsymbol{r}) = \int \frac{d^2 k_T}{k_T^4} \phi(y, k_T)(1 - e^{i\boldsymbol{k}_T \cdot \boldsymbol{r}}),$$
$$xg(x, \mu_F) = \int_0^{\mu_F} \frac{d^2 k_T}{k_T^2} \phi(x, k_T), \tag{4}$$

where $y = \ln(1/x)$. Equation (4) might be inverted and gives the gluon PDF in terms of the dipole amplitude as follows:

$$xg(x, \mu_F) = \frac{C_F \mu_F}{2\pi^2 \bar{\alpha}_S} \int d^2 r \frac{J_1(r\mu_F)}{r} \nabla_r^2 N(y, \boldsymbol{r}). \tag{5}$$

This result allows us to rewrite Eq. (1) entirely in terms of the dipole amplitude N.

Now we would like to briefly describe this process in the BFKL framework. While we use the dipole framework for our evaluations, it is known that the dipole scattering amplitude resums certain classes of BFKL Pomeron contributions, and for this reason understanding the dominant contributions in the BFKL picture could help us to clarify certain features of the cross sections. The inclusive production of P-wave quarkonia in the BFKL picture gets its dominant contribution from the fusion of two Pomerons, as shown in the left panel of Fig. 2. However, as was suggested in analyses of similar processes in [25–30], at large multiplicities this contribution might be supplemented by the three-Pomeron fusion shown in the right panel of Fig. 2. While formally it is expected that such contributions would be suppressed in the heavy quark mass limit, numerically this suppression might not be very strong, due to enhanced gluon densities in the small-x kinematics. As was demonstrated in [25,26], this indeed happens in the case of $1S$ charmonia production, and the multi-Pomeron contributions are especially important in events with large multiplicities of coproduced hadrons. From the quantum numbers of P-wave quarkonia and the symmetry properties of its wave function, we can see that such a contribution is suppressed at high energies since it requires antisymmetrization over color indices of both Pomerons. Similarly, in the BFKL picture the contributions of multi-Reggeon states made of several interconnected gluon ladders [73,74] should be negligible because such configurations have smaller intercepts and are suppressed at high energies [75]. For this reason in LHC kinematics we may disregard

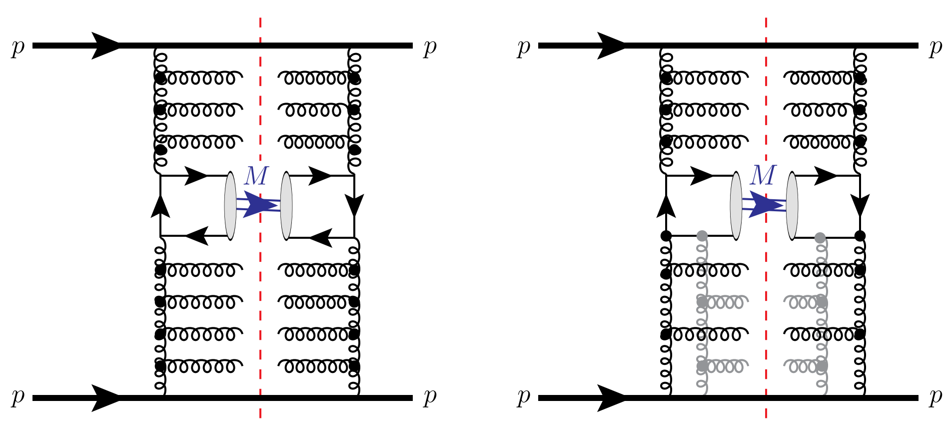

FIG. 2. P-wave quarkonia production in the BFKL picture. Left panel: leading order contribution to the cross section of P-wave meson production via the two-Pomeron fusion mechanism. The diagram includes two cut Pomerons (gluon ladders split by a unitarity cut). Right panel: possible contributions of the three-Pomeron mechanism. In the inferior part of the diagram we show one of the Pomerons (gluon ladder split by a unitarity cut) in gray. In both plots the vertical dashed line represents unitarity cuts. The produced meson M is shown with a double line and arrow. A summation over all possible permutations of gluon vertices in the heavy quark line/loop is implied.

higher order contributions like those shown in the right panel of Fig. 2.

Finally, we would like to briefly discuss possible contributions of the color octet mechanism [1–7], which might be relevant in the large-p_T kinematics. For P-wave quarkonia the color octet contribution is controlled by the LDME $\mathcal{O}^{\chi_c}[^3S_1^{(8)}]$. The analyses available from the literature [35–37] conclude that the value of this LDME is very small, although the estimates of its exact value vary significantly from 4.78×10^{-5} to 2.01×10^{-3} GeV^3. In view of these findings, in what follows we will simply omit the contribution of the color octet mechanism.

III. NUMERICAL ESTIMATES

In the CGC/Sat approach, the dipole amplitude $N(y,\vec{r},\vec{b})$ is expected to satisfy the nonlinear Balitsky-Kovchegov equation [60,61,76] for the dipoles of small size r. In the saturation region this solution should exhibit a geometric scaling, being a function of one variable $\tau = r^2Q_s^2$, where Q_s is the saturation scale [77–80]. Such behavior is implemented in different phenomenological parametrizations available in the literature. One of such parametrizations which we will use for our numerical estimates is the CGC parametrization, which was proposed in [81] (see also [82–85] for more recent phenomenological analyses),

$$N(x,\vec{\boldsymbol{r}}) = \sigma_0 \times \begin{cases} N_0\left(\frac{rQ_s(x)}{2}\right)^{2\gamma_{\mathrm{eff}}(r)}, & r\le\frac{2}{Q_s(x)} \\ 1-\exp(-\mathcal{A}\ln(\mathcal{B}rQ_s)), & r>\frac{2}{Q_s(x)} \end{cases}, \tag{6}$$

$$\mathcal{A} = -\frac{N_0^2\gamma_s^2}{(1-N_0)^2\ln(1-N_0)}, \qquad \mathcal{B} = \frac{1}{2}(1-N_0)^{-\frac{1-N_0}{N_0\gamma_s}}, \tag{7}$$

$$Q_s(x) = \left(\frac{x_0}{x}\right)^{\lambda/2}, \qquad \gamma_{\mathrm{eff}}(r) = \gamma_s + \frac{1}{\kappa\lambda Y}\ln\left(\frac{2}{rQ_s(x)}\right), \tag{8}$$

$$\gamma_s = 0.762, \qquad \lambda = 0.2319,$$
$$\sigma_0 = 21.85\ \mathrm{mb}, \qquad x_0 = 6.2\times10^{-5}, \tag{9}$$

$$Y = \ln(1/x). \tag{10}$$

We would like to start our discussion of results with a comparison of the predicted p_T dependence of the cross sections with experimental data. The cross section of χ_c production is smaller than the cross section of J/ψ; for this reason there are many fewer experimental data available from the literature. Since χ_{cJ} is usually detected via the $\chi_{cJ}\to\gamma+J/\psi$ radiative decay channel, the experimental data are traditionally presented for the product of the cross section onto the branching fraction $\mathcal{B}(\chi_{cJ})\equiv \mathrm{Br}(\chi_{cJ}\to\gamma+J/\psi)Br(J/\psi\to\mu^+\mu^-)$. For the χ_{bJ} mesons we use a similar product of branching fractions with $\Upsilon(1S)$ instead of J/ψ. The values of the branching fractions are known from [86] and for the sake of completeness are shown in Table I. As we can see, the values of $\mathcal{B}(\chi_{c0})$ and $\mathcal{B}(\chi_{b0})$ are extremely small compared to the other channels. For this reason observation of these states via radiative decays into $1S$ quarkonia is very difficult, and all the available data are given for χ_{c1} and χ_{c2} mesons.

In Figs. 3 and 4 we compare the model predictions for the χ_{cJ} production with available data from ATLAS [87], CMS [88], LHCb [89], and CDF [90]. We can see that the CGC/Sat model provides a reasonable description of the available data in a wide kinematic range and thus might be used for further analysis.

In Fig. 5 we show the p_T dependence of the cross sections at different values of the collision energies $\sqrt{s}$, which might be relevant for future experimental data. In the large-p_T kinematics we expect that the cross section will increase as a function of energy without changing the shape of p_T dependence. To illustrate the dependence on the choice of wave function ($\sim$ the potential model used for its evaluation), we have also shown in Fig. 5 the ratio of the cross sections evaluated with Cornell [92,93] and powerlike [94] parametrizations of the rest frame potential. While the cross sections change several orders of magnitude in the considered range of p_T, the uncertainty due to choice of the potential does not exceed 15%. We got similar estimates for the parametrization [95]. The cross sections of χ_{c0} and χ_{c2} get large contributions from the configuration with aligned spins of the quarks, whereas in the case of χ_{c1} there is also a sizable contribution from configurations where spins are antialigned, which explains the difference.

In Fig. 6 we show our predictions for the p_T dependence of χ_{b1} and χ_{b2} mesons. The estimated cross sections are smaller than those of the χ_{c1} and χ_{c2} mesons, although they are within the reach of LHC experiments. Thus far there have been no published data from LHC for the cross sections of these mesons, but we hope that in the near future such measurements will be carried out.

IV. MULTIPLICITY DEPENDENCE

As we found in the previous section, the CGC/Sat model (1) provides a reasonable description of the χ_{c1}

TABLE I. Values of the product of branching fractions $\mathcal{B}(\chi_{cJ})\equiv \mathrm{Br}(\chi_{cJ}\to\gamma+J/\psi)\mathrm{Br}(J/\psi\to\mu^+\mu^-)$ and $\mathcal{B}(\chi_{bJ})\equiv\mathrm{Br}(\chi_{cJ}\to\gamma+\Upsilon(1S))\mathrm{Br}(\Upsilon(1S)\to\mu^+\mu^-)$, as given in [86].

	$J=0$	$J=1$	$J=2$
$\mathcal{B}(\chi_{cJ})$	0.08%	2.02%	1.12%
$\mathcal{B}(\chi_{bJ})$	0.05%	0.87%	0.44%

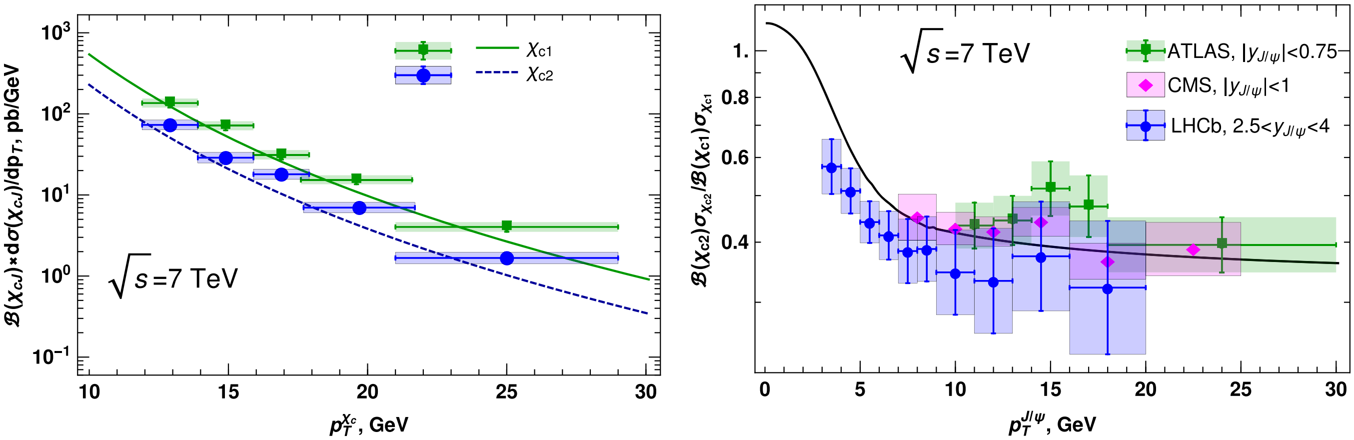

FIG. 3. Left panel: comparison of the predicted p_T dependence for the χ_{c1} and χ_{c2} cross sections. Experimental data are from ATLAS [87]. Right panel: comparison of the model predictions for the ratio of χ_{c1} and χ_{c2} cross sections at central rapidities, with experimental data from the ATLAS [87], CMS [88], and LHCb [89] experiments. We added for comparison the LHCb data measured at off-forward rapidities because we expect that the suppression of the cross sections of χ_{c1} and χ_{c2} production at off-forward rapidities will be the same and thus will cancel in the ratio. For better visibility we use a logarithmic scale in the vertical axis.

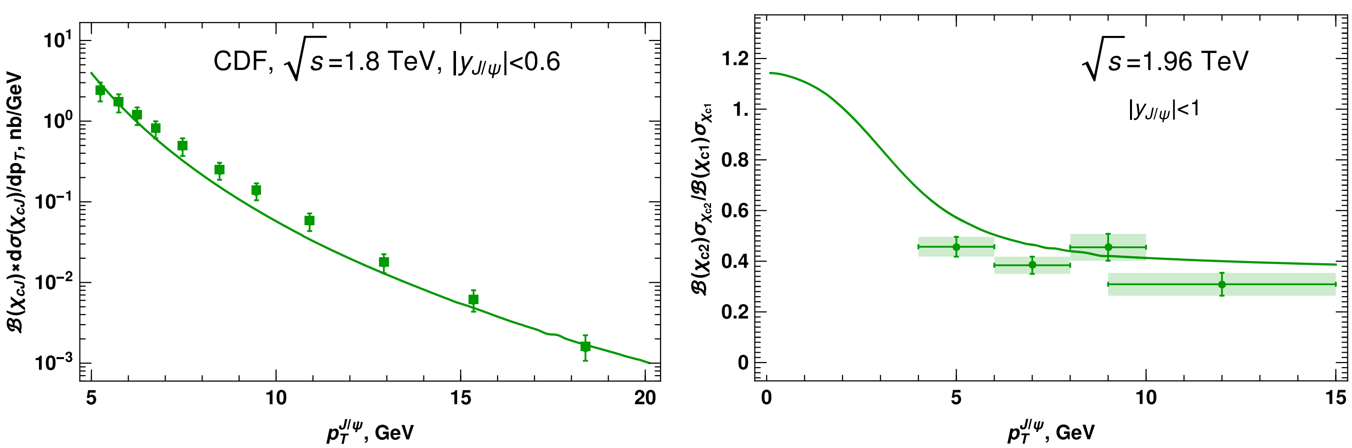

FIG. 4. Left panel: comparison of the predicted $p_T^{J/\psi}$ dependence for χ_c meson production with experimental data from CDF [90] at central rapidities ($|y| < 1$). Right panel: comparison of model predictions for the ratio of the χ_{c2} and χ_{c1} cross sections to experimental data from [91].

and χ_{c2} production data at Tevatron and LHC kinematics. The description of the multiplicity dependence presents more challenges at the conceptual level because there are different mechanisms to produce an enhanced number of charged particles $N_{\rm ch}$. Historically the studies of multiplicities were initiated long ago in [19–24] in the framework of the Regge approach. Using only rather general properties of particle-Reggeon vertices, which are largely independent of the underlying quantum field theory, it was found that in high energy processes multiple Pomeron exchanges might lead to various observable effects in multiparticle final states like fluctuations of the rapidity densities of produced particles, long-range rapidity correlations, and an increase of multiplicity in the final state. As was demonstrated in [56,63,66,96–98], all these findings are also valid in the context of QCD, and they have been confirmed by experimental evidence.

The probability of multiplicity fluctuations decreases rapidly as a function of the number of produced charged particles $N_{\rm ch}$ [99]; therefore, for the study of multiplicity dependence it is more common to use a self-normalized ratio [17]

$$\frac{dN_M/dy}{\langle dN_M/dy\rangle} = \frac{w(N_M)}{\langle w(N_M)\rangle}\frac{\langle w(N_{\rm ch})\rangle}{w(N_{\rm ch})} = \frac{d\sigma_M(y,\eta,\sqrt{s},n)/dy}{d\sigma_M(y,\eta,\sqrt{s},\langle n\rangle = 1)/dy}\Bigg/\frac{d\sigma_{\rm ch}(\eta,\sqrt{s},Q^2,n)/d\eta}{d\sigma_{\rm ch}(\eta,\sqrt{s},Q^2,\langle n\rangle = 1)/d\eta}, \tag{11}$$

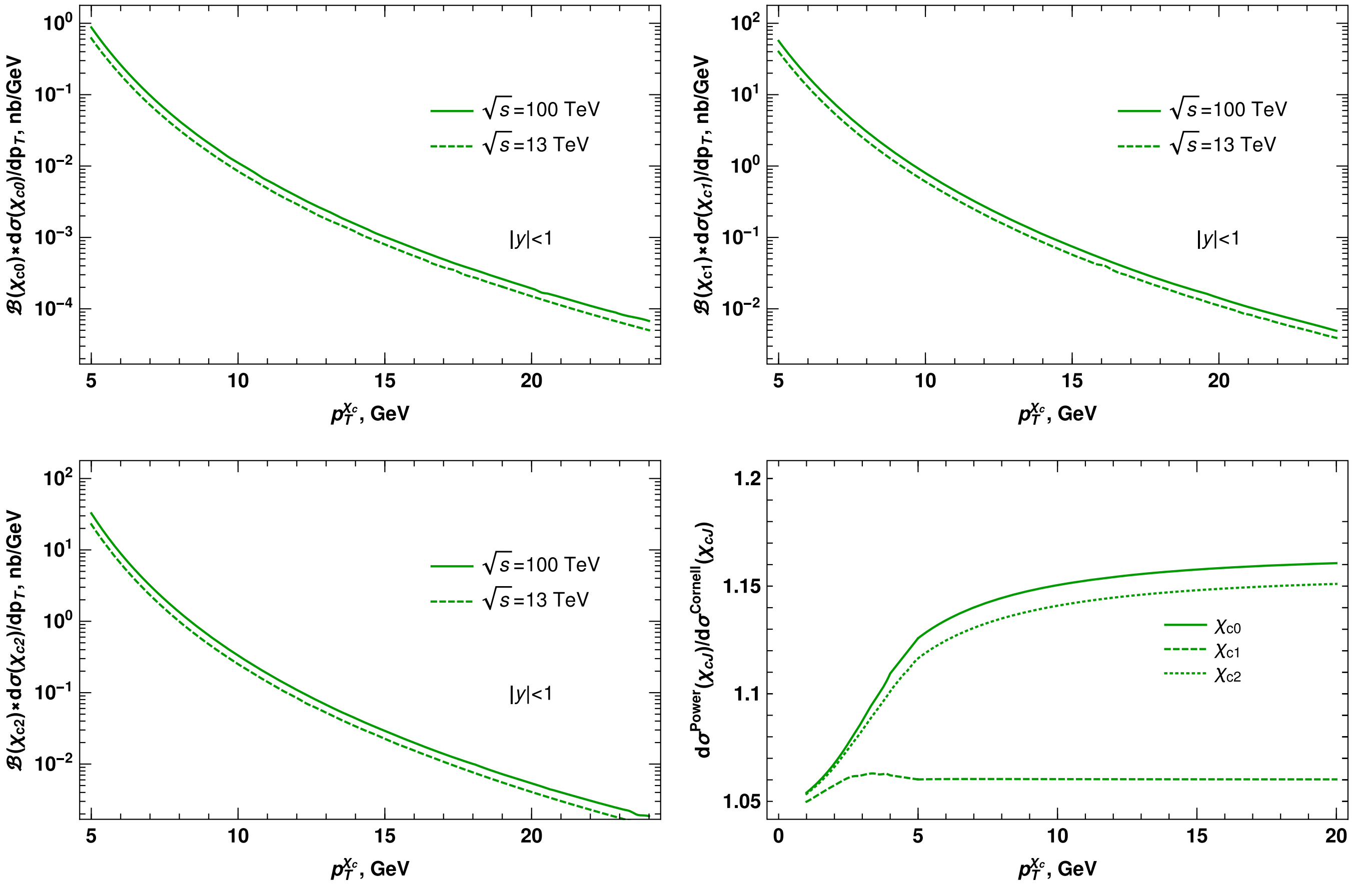

FIG. 5. Upper row and left panel of lower row: comparison of the predicted p_T dependence for the χ_{c0}, χ_{c1}, and χ_{c2} cross sections for different values of $\sqrt{s}$. All the theoretical curves are shown multiplied by the branching $\mathcal{B}(\chi_{cJ}) \equiv \mathrm{Br}(\chi_{cJ} \to \gamma + J/\psi)\mathrm{Br}(J/\psi \to \mu^+\mu^-)$. The cross sections for χ_{c0} are strongly suppressed relative to χ_{c1} and χ_{c2} due to differences in the branching fractions $\mathrm{Br}(\chi_{cJ} \to \gamma + J/\psi)$. Lower right panel: ratio of cross sections evaluated with Cornell [92,93] and powerlike [94] parametrizations of the potential (see Appendix B for more details).

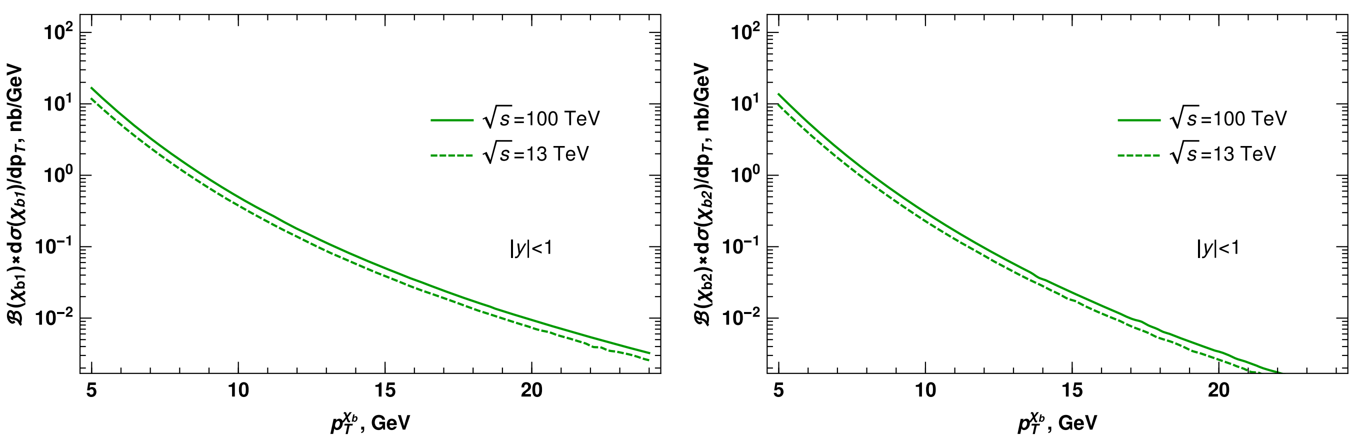

FIG. 6. The p_T dependence for χ_{b1} and χ_{c2} cross sections for different values of $\sqrt{s}$. All the theoretical curves are shown multiplied by the branching $\mathcal{B}(\chi_{bJ}) \equiv \mathrm{Br}(\chi_{bJ} \to \gamma + \Upsilon)\mathrm{Br}(\Upsilon \to \mu^+\mu^-)$.

where $n = N_{\rm ch}/\langle N_{\rm ch}\rangle$ is the relative enhancement of the charged particles in the bin, $w(N_M)/\langle w(N_M)\rangle$ and $w(N_{\rm ch})/\langle w(N_{\rm ch})\rangle$ are the self-normalized yields of quarkonium M and charged particles (minimal bias) events in a given multiplicity class, and $d\sigma_M(y, \sqrt{s}, n)$ is the production cross section for M, with rapidity y and $\langle N_{\rm ch}\rangle = \Delta\eta dN_{\rm ch}/d\eta$ charged particles in the pseudorapidity window $(\eta - \Delta\eta/2, \eta + \Delta\eta/2)$. If the inclusive cross section of the process $pp \to M + X$ is proportional to the probability of producing a meson M in a single pp collision, then the ratio (11) gives the *conditional* probability of producing a meson M in a pp collision in which $N_{\rm ch}$ charged particles are produced. In what follows we are going to focus only on multiplicity dependence in pp collisions for moderate values of $n \lesssim 10$. In this kinematics due to the local parton-hadron duality hypothesis [100–102], the number of produced charged particles is directly proportional to the number of partons which stem from the individual Pomerons and thus might be studied using perturbative methods. For AA collisions this hypothesis might not work due to formation of the quark-gluon plasma at later stages of collisions [103–117], and the suggested approach should instead be replaced with hydrodynamic models.

In the color dipole approach used in this paper, the multiplicity dependence should be encoded in the dipole amplitude. We expect that even in high-multiplicity events the dipole amplitude still should satisfy the nonlinear Balitsky-Kovchegov equation, and therefore might be described by Eq. (6), although the value of the saturation scale Q_s might be modified. As was demonstrated in [52–54], the observed number of charged multiplicity $dN_{\rm ch}/dy$ of soft hadrons in pp collisions is given by

$$\frac{dN_{\rm ch}}{dy} = c\frac{Q_s^2}{\bar{\alpha}_S(Q_s^2)}, \tag{12}$$

where c is a numerical coefficient. Solving Eq. (12) algebraically, we could extract Q_s^2 as a function of $dN_{\rm ch}/dy$. Taking into account the fact that the distribution $dN_{\rm ch}/dy$ is almost flat, we may approximate $n = N_{\rm ch}/\langle N_{\rm ch}\rangle \approx (dN_{\rm ch}/dy)/\langle dN_{\rm ch}/dy\rangle$, so Eq. (12) allows us to express Q_s^2 as a function of n. Usually in the literature the logarithmic dependence on n, which stems from the running coupling in the denominator of Eq. (12), is disregarded, so Eq. (12) reduces to a simpler linearly growing dependence on n [52–59],

$$Q_s^2(x, b; n) = nQ^2(x, b). \tag{13}$$

The precision of this assumption was tested in [59], and it was found that a numerical solution of the running coupling Balitsky-Kovchegov equation differs from Eq. (13) by less than 10% in the region of interest ($n \lesssim 10$). This correction is within the precision of current evaluations, and for this reason in what follows we will use Eq. (13) for our estimates. While at LHC energies it is expected that the typical values of saturation scale $Q_s(x, b)$ would fall into the range 0.5–1 GeV, from Eq. (13) we can see that in events with enhanced multiplicity this parameter might exceed the values of heavy quark mass m_Q and lead to an interplay of large-Q_s and large-m_Q limits. Since increase of multiplicity and increase of energy (decrease of x) affect Q_s^2 in a similar way, the study of the high-multiplicity events allows one to study a deeply saturated regime which determines the dynamics of all processes at significantly higher energies.

As was discussed in [25,26,30], for studies of multiplicity dependence it is important that the experimental setup allow one to distinguish the charged particles produced with rapidity above or below that of quarkonia (eventually, this will determine the fraction of multiplicity enhancement which should be attributed to each dipole amplitude). For phenomenological estimates we shall focus on the setup in which both quarkonia and hadrons are

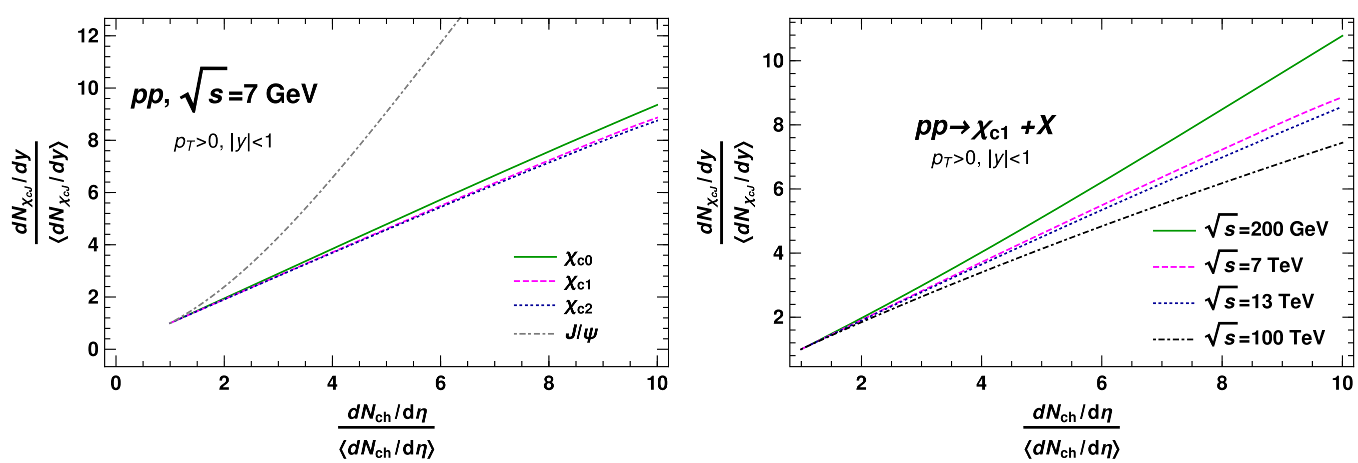

FIG. 7. Left panel: multiplicity dependence for different χ_{cJ} states. While the cross sections differ quite significantly due to spin structure, the self-normalized ratios are very close to each other. For the sake of reference we also added a dot-dashed gray curve for J/ψ production from our previous work [25,26]. Right panel: dependence of the multiplicity shapes on collision energies $\sqrt{s}$. The plot is done for χ_{c1} meson production, but the results for χ_{c0} and χ_{c2} are almost identical. All evaluations are done while assuming that charged particles and quarkonia have been collected at central rapidities ($|\eta, y| < 1$), which is similar to what is available for J/ψ production from [12].

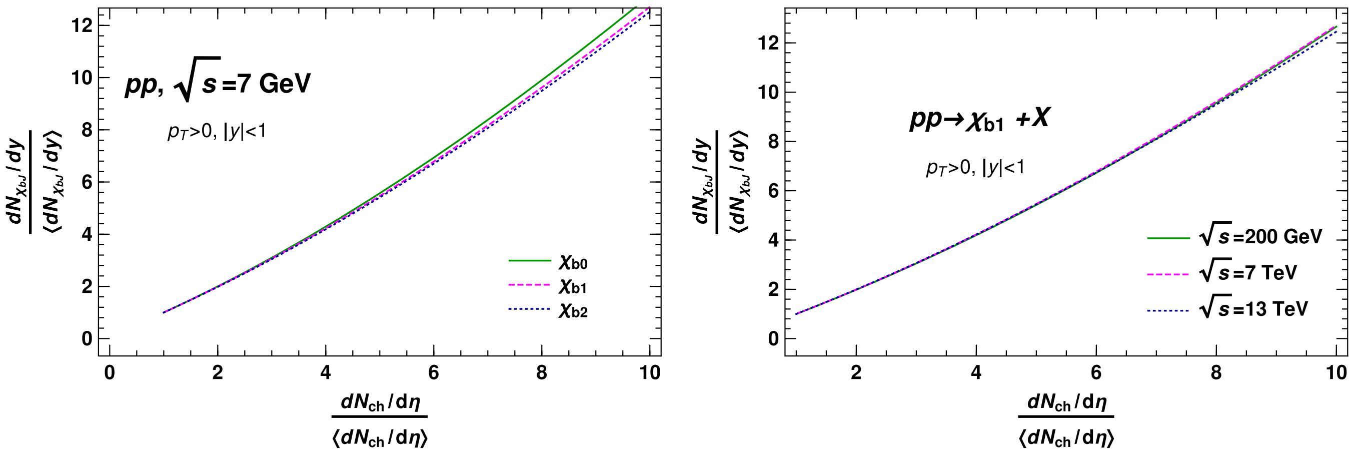

FIG. 8. Left panel: multiplicity dependence for different χ_{bJ} states. While the cross sections differ quite significantly due to spin structure, the self-normalized ratios are very close to each other. Right panel: dependence of the multiplicity shapes on collision energies $\sqrt{s}$. The plot is done for χ_{b1} meson production, but results for χ_{b0} and χ_{b2} are almost identical. All evaluations are done while assuming that charged particles and quarkonia have been collected at central rapidities ($|\eta, y| < 1$), which is similar to what is available from [12].

collected at central rapidities $|\eta|, |y| \leq 1$, where the strongest multiplicity dependence was observed for J/ψ and D mesons. In Fig. 7 and 8 we show the multiplicity dependence of χ_{cJ} and χ_{bJ} mesons for different energies. As we can see, the dependence is much milder than that of the $1S$ quarkonia (dot-dashed curve with label "J/ψ"). This dependence agrees with our earlier expectations based on the BFKL picture and the dominance of the two-Pomeron mechanism. Indeed, in that picture each cut Pomeron contributes to the multiplicity dependence factor $\sim n^{\langle\gamma_{\rm eff}\rangle}$, where the parameter $\gamma_{\rm eff}$ is defined in Eq. (8). Since χ_b has a smaller size than χ_c, the typical values of $\langle\gamma_{\rm eff}\rangle$ are larger for the former than for the latter, and χ_b has slightly a faster dependence on multiplicity than χ_c. Similarly, we can understand the change of multiplicity dependence with energy: due to the prefactor $1/Y$ in Eq. (8), the average values of the parameter $\langle\gamma_{\rm eff}\rangle$ *decrease* as a function of $\sqrt{s}$, and for this reason the dependence on multiplicity becomes milder for larger energies $\sqrt{s_{pp}}$.

V. CONCLUSIONS

In this paper we analyzed in detail the production of χ_c and χ_b mesons in the CGC/Sat approach. We found that the model predictions for the p_T-dependent cross section are in agreement with available experimental data for χ_{c1} and χ_{c2} mesons in LHC kinematics. We also made predictions for χ_b mesons, which might be checked in the ongoing and future experiments, both at RHIC and at LHC. We also studied the dependence of the cross sections on the multiplicity of coproduced hadrons and found that it is significantly milder than that of $1S$ quarkonia ($J/\psi, \Upsilon \cdots$). This effect is quite easy to understand in the BFKL picture: the dominant production mechanism for the P-wave quarkonia is the two-Pomeron fusion, whereas the three-Pomeron contributions are strongly suppressed at high energies. Our evaluation is largely parameter-free and relies only on the choice of the parametrization for the dipole cross section (6) and the wave function of the meson.

The explanation of multiplicity dependence in the CGC/Sat approach differs from other approaches suggested for the description of multiplicity dependence, like the percolation approach [118] or modification of the slope of the elastic amplitude [119]. While for $1S$ quarkonia all approaches give comparable descriptions, this is not so for P-wave quarkonia. For this reason we expect that the measurement of the multiplicity dependence of χ_c and χ_b would be an important litmus test for all the models which describe production of quarkonia, and we hope that it will be done at both LHC and RHIC.

ACKNOWLEDGMENTS

We thank our colleagues at UTFSM university for encouraging discussions. This research was partially supported by Project No. ANID PIA/APOYO AFB180002 (Chile) and Fondecyt (Chile) Grant No. 1180232. We also thank Yuri Ivanov for the technical support of the USM HPC cluster, where some evaluations were performed.

APPENDIX A: EVALUATION OF THE DIPOLE AMPLITUDES

In this Appendix, for the sake of completeness, we explain the main technical steps and assumptions used for the derivation of the cross section (1). The general rules, which allow one to express the cross sections of hard processes in terms of the color singlet dipole cross section, can be found in [43–51]. While technically the rules might differ at intermediate steps, they eventually reproduce equivalent expressions. For the sake of definiteness we will follow the procedure and notations developed in [50,51], which include a simple derivation of the $\bar{Q}Q$ production cross sections. In the heavy quark mass limit the strong coupling $\alpha_s(m_Q)$ is small, so the interaction of a heavy $\bar{Q}Q$ dipole with gluons might be considered perturbatively. At the same time, we tacitly assume that each such gluon should be understood as a parton shower ("Pomeron"). The process of P-wave quarkonia production differs from equivalent production of open heavy flavor mesons only by an additional projection on the Hilbert state of the final meson $\mathcal{M}$.

In the high energy eikonal picture, the interaction of the quark and antiquark with a t-channel gluon does not change helicities of fermions, and for this reason it might be described by a factor $\pm igt^a\gamma_a(\boldsymbol{x}_\perp)$, where $\boldsymbol{x}_\perp$ is the transverse coordinate of the quark and the nonperturbative function $\gamma_a(\boldsymbol{x}_\perp)$ characterizes the distribution of gluons in the target in the transverse plane. This function is related to a dipole scattering amplitude $N(x,\boldsymbol{r})$ probed in deep inelastic scattering as

$$N(x,\boldsymbol{r}) = \frac{1}{8}\int d^2b|\gamma_a(x,\boldsymbol{b}-z\boldsymbol{r}) - \gamma_a(x,\boldsymbol{b}+\bar{z}\boldsymbol{r})|^2, \tag{A1}$$

where $\boldsymbol{r}$ is the transverse size of the dipole and z is the light-cone fraction of the dipole momentum carried by the quarks. Equation (A1) has a very simple structure and might be obtained by taking traces over color matrices in diagrams with a single gluon attachment in amplitude and its conjugate.

In the Iancu-Mueller approach [120] (see also [52]) it was shown that interaction of the dipole with the target is described by the S-matrix element

$$S(\boldsymbol{x},\boldsymbol{y}) = \frac{1}{N_c}\langle V^\dagger(\boldsymbol{x})V(\boldsymbol{y})\rangle, \tag{A2}$$

where $y = \ln(1/x)$ is the rapidity of the dipole and $V^\dagger(\boldsymbol{x})$ and $V(\boldsymbol{y})$ are Wilson lines describing the scattering of the quark and antiquark with transverse coordinates $\boldsymbol{x}, \boldsymbol{y}$ in the color field of a hadron. The dipole amplitude $N(x,\boldsymbol{r})$ is related to $S(y,\boldsymbol{x},\boldsymbol{y})$ as

$$N(x,\boldsymbol{r}) = 1 - S(y,\boldsymbol{x},\boldsymbol{y}). \tag{A3}$$

As we discussed earlier, for heavy flavors we may expect that the interaction of a dipole with a gluonic field becomes perturbative, so we can see that Eqs. (A2) and (A3) might be approximated in this limit by Eq. (A1) provided that $\gamma_a(\boldsymbol{x})$ is identified with gluonic field $A_a^+(\boldsymbol{x})$. However, we would like to emphasize that the heavy quark limit suppression does not work for possible couplings in virtual loop corrections, and for this reason the evolution of the dipole amplitude is still described by the nonlinear Balitsky-Kovchegov equation.

Equation (A1) can be rewritten in the form

$$\frac{1}{8}\int d^2\boldsymbol{b}\gamma_a(x,\boldsymbol{b})\gamma_a(x,\boldsymbol{b}+\boldsymbol{r}) = \frac{1}{2}N(x,\boldsymbol{r}) + \underbrace{\int d^2b|\gamma_a(x,\boldsymbol{b})|^2}_{=\text{const}}. \tag{A4}$$

The value of the constant term in the right-hand side of Eq. (A4) is related to the infrared behavior of the theory, and for the observables which we consider in this paper it cancels exactly. For very small dipoles, the dipole scattering amplitude $N(x,r)$ is related to the gluon uPDF as [121]

$$N(x,\vec{r}) = \frac{4\pi\alpha_s}{3}\int\frac{d^2k_\perp}{k_\perp^2}\mathcal{F}(x,k_\perp)(1-e^{ik\cdot r}) + \mathcal{O}\left(\frac{\Lambda_{\mathrm{QCD}}}{m_c}\right), \tag{A5}$$

so the functions $\gamma_a(x,\boldsymbol{r})$ might also be related to the unintegrated gluon densities in coordinate space. With the help of Eq. (A4), it is possible to express the production cross sections of some processes as linear combinations of the dipole amplitudes $N(x,\boldsymbol{r})$ with different arguments. A cautious reader might note that such relations still rely on the assumption that the interaction of the gluon shower with a quark is described by the same color generator t_a as the single perturbative gluon. This merely reflects our earlier assumption that the interactions of gluons *with heavy quarks* is perturbative, even in the deeply saturated regime.

For the case of P-wave production, the dominant contribution to the process is due to the color singlet mechanism; namely, it occurs only with $\bar{Q}Q$ states in color singlet color state. For this reason in evaluations we should take into account Figs. 9(a) and 9(b) only. While the color

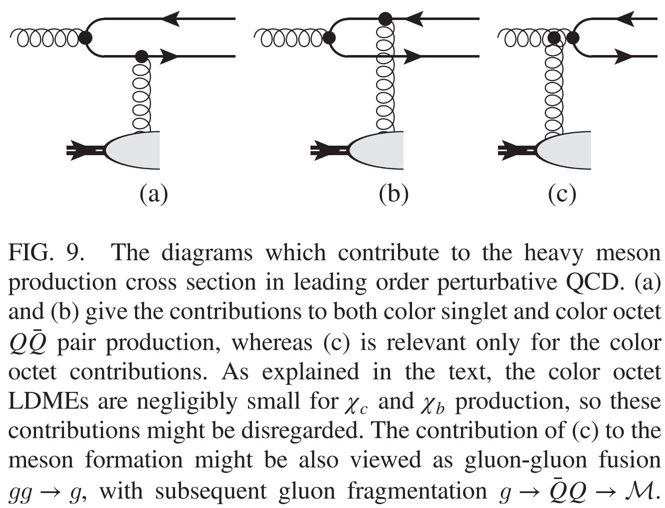

FIG. 9. The diagrams which contribute to the heavy meson production cross section in leading order perturbative QCD. (a) and (b) give the contributions to both color singlet and color octet $Q\bar{Q}$ pair production, whereas (c) is relevant only for the color octet contributions. As explained in the text, the color octet LDMEs are negligibly small for χ_c and χ_b production, so these contributions might be disregarded. The contribution of (c) to the meson formation might be also viewed as gluon-gluon fusion $gg \to g$, with subsequent gluon fragmentation $g \to \bar{Q}Q \to \mathcal{M}$. In the CGC approach t-channel gluons are replaced by the dipole amplitude which satisfies the Balitsky-Kovchegov equation and corresponds to a fanlike shower of soft particles in the diagrammatic language.

octet mechanism potentially might also make a contribution, it is known from the literature that for χ_c and χ_b production the corresponding LDMEs are very small [35–37] and might be neglected. As we showed in Sec. III, the color singlet model alone gives a very plausible description of the data, which indirectly signals that the omission of the color singlet contribution is justified. After a straightforward evaluation of traces and color indices it is possible to get for the square of the amplitude in the color singlet mechanism

$$|\mathcal{A}_{gp\to\mathcal{M}(\boldsymbol{p}_T)X}|^2 \sim \int dz_1 dz_2 d^2\boldsymbol{r}_1 d^2\boldsymbol{r}_2 \int d^2\boldsymbol{b}_{21} d^2\boldsymbol{b} e^{-i\boldsymbol{p}_T\cdot\boldsymbol{b}_{21}} \langle \Psi^\dagger_{\bar{Q}Q}(r_2,z_2)\Psi_M(r_2,z_2)\rangle^* \langle \Psi^\dagger_{\bar{Q}Q}(r_1,z_1)\Psi_M(r_1,z_1)\rangle \times (\gamma_a(\boldsymbol{b}+\bar{z}_2\boldsymbol{r}_2)-\gamma_a(\boldsymbol{b}-z_2\boldsymbol{r}_2))^*(\gamma_a(\boldsymbol{b}+\bar{z}_1\boldsymbol{r}_1)-\gamma_a(\boldsymbol{b}-z_1\boldsymbol{r}_1)), \tag{A6}$$

where $(z_i,\boldsymbol{r}_i)$ represent the fraction of the dipole momentum carried by the quark and the size of the dipole, $\boldsymbol{b}_i$ is the impact parameter of the dipole, and the subscript index i might take values $i=1,\ 2$ to distinguish between the variable in the amplitude and its conjugate. In the arguments of γ we have the quark and antiquark transverse coordinates are given by $\boldsymbol{b}_i - z_i\boldsymbol{r}_i$ and $\boldsymbol{b}_i+\bar{z}_i\boldsymbol{r}_i$, respectively. For the evaluation of the p_T-dependent cross section we need to project the coordinate space quark distribution onto the state with definite transverse momentum $\boldsymbol{p}_T$, so we have to evaluate the additional convolution $\sim\int d^2\boldsymbol{b}_1 d^2\boldsymbol{b}_2 e^{i\boldsymbol{p}_T\cdot(\boldsymbol{b}_1-\boldsymbol{b}_2)} \equiv \int d^2\boldsymbol{b}_{21} d^2\boldsymbol{b} e^{-i\boldsymbol{p}_T\cdot\boldsymbol{b}_{21}}$, where $\boldsymbol{b}_{21}\equiv \boldsymbol{b}_2-\boldsymbol{b}_1$ is the difference of impact parameters of the dipole center of mass in the amplitude and its conjugate and $\boldsymbol{b}=(\boldsymbol{b}_1+\boldsymbol{b}_2)/2$. After some trivial algebraic simplifications and using Eq. (A4) for evaluation of the integral over $\int d^2\boldsymbol{b}$, we can get the result in the form of Eq. (1).

All evaluations of this appendix were done in the frame where the momentum of the primordial gluon is zero. In any other frame we should take into account an additional convolution with the momentum distribution of the incident ("primordial") gluons, as appears in the first line of Eq. (1).

APPENDIX B: WAVE FUNCTIONS

For evaluations of Eq. (1), we will need explicit parametrizations for the $\bar{Q}Q$ component of the light-cone gluon wave function $\Psi_{\bar{Q}Q}$ and the P-wave quarkonia wave function Ψ_M. We may expect that in the heavy quark mass limit for $\Psi_{\bar{Q}Q}$ we may use the well-known perturbative expressions available in the literature [122,123],

$$\Psi^{(+1)}_{\bar{Q}Q}(z,\boldsymbol{r}) = \frac{\sqrt{2N_c}}{2\pi}(ie^{i\theta}\varepsilon(z\delta_{h+}\delta_{\bar{h}-}-(1-z)\delta_{h-}\delta_{\bar{h}+})K_1(\varepsilon r)+m_Q\delta_{h+}\delta_{\bar{h}+}K_0(\varepsilon r)),$$
$$\Psi^{(-1)}_{\bar{Q}Q}(z,\boldsymbol{r}) = \frac{\sqrt{2N_c}}{2\pi}(ie^{-i\theta}\varepsilon((1-z)\delta_{h+}\delta_{\bar{h}-}-z\delta_{h-}\delta_{\bar{h}+})K_1(\varepsilon r)+m_Q\delta_{h-}\delta_{\bar{h}-}K_0(\varepsilon r)), \tag{B1}$$

where the superscript index (±1) of $\Psi_{\bar{Q}Q}$ refers to helicity of the projectile gluon, and $h,\bar{h}$ in the rhs are the helicities of the quark and antiquark, respectively.

Most previous evaluations of quarkonia production [35–41] were done in the heavy quark mass limit under the assumption that the wave function $\Psi_M(z,\boldsymbol{r})$ might be approximated with its small-$\boldsymbol{r}$ Taylor expansion, which starts with a linear term for the P-wave. In this case the dependence on the wave function reduces to dependence on the value of the slope $|\mathcal{R}'(0)|$. This scheme is justified in the heavy quark mass limit. However, it is clear that for charmonia the heavy quark mass limit might not work very well, and for this reason we will maintain the full r dependence of the wave function.

For our evaluations we construct a light-cone wave function from the rest frame wave functions evaluated in the potential models using the Brodsky-Huang-Lepage (BHL) prescription [124] (see also [125] for a similar scheme). It is known that for heavy quarkonia the results of the BHL prescription are close to the wave functions evaluated in Covariant Spectator Theory (CST) [126] as well as lattice evaluations [127–129]. According to BHL prescription, the light-cone wave function is related to the rest frame wave function as [124,130,131]

$$\Phi_{\rm LC}(z,r) = \sqrt{N_c}\int d^2k_\perp e^{ik_\perp\cdot r_\perp}\left(\frac{k_\perp^2+m_Q^2}{2z^3(1-z)^3}\right) \times \psi_{\rm RF}\left(\sqrt{\frac{k_\perp^2+(1-2z)^2m_Q^2}{4z(1-z)}}\right), \tag{B2}$$

where $\psi_{\rm RF}(\boldsymbol{k})$ is the Fourier image of the rest frame wave function. Owing to the spin-orbital interaction, we expect that the spinorial structure of the wave functions of χ_{cJ},χ_{bJ} will crucially depend on the angular momentum J, and for this reason the production cross sections of χ_{cJ} and χ_{bJ} mesons will acquire dependence on J [132].

The rest frame quarkonium wave function might be written using the Clebsch-Gordan coefficients as

$$\langle \boldsymbol{r}|J,J_z\rangle = \sum_{S=0}^{1}\sum_{M+S_z=J_z}\sum_{s_1+s_2=S_z}\chi_{s_1}\bar{\chi}_{s_2}\left\langle S,S_z\Big|\frac{1}{2},s_1;\frac{1}{2},s_2\right\rangle \times \langle J,J_z|1,M;S,S_z\rangle \mathcal{R}_{n1}(r)Y_{1M}(\hat{\boldsymbol{r}}),$$

where $\{\chi_s\}$ are spinors corresponding to definite projection of spin s of the quark and antiquark, M is the projection of orbital angular momentum, $\mathcal{R}_{n1}(r)$ is the radial wave function of the P-wave quarkonium, and Y_{1M} is an ordinary spherical harmonic. A set of useful relations between Clebsch-Gordan coefficients, which facilitate the summations, can be found in [36,42]. For the evaluations of radial part $\mathcal{R}_{n1}$ we used expressions found in potential models. For the sake of comparison in evaluation we consider three different choices of the potential:

(i) The Cornell potential which was introduced in [92,93],

$$V_{\mathrm{Cornell}}(r) = -\frac{\alpha}{r} + \sigma r. \tag{B3}$$

(ii) The potential with the logarithmic large-r behavior suggested in [95],

$$V_{\mathrm{Log}}(r) = \alpha + \beta \ln r. \tag{B4}$$

TABLE II. Values of the slope $|\mathcal{R}'(0)|^2$ evaluated with different models of interquark potential interaction.

	Cornell (B3)	Log (B4)	Power (B5)
$\lvert\mathcal{R}'(0)\rvert^2$, [GeV^5]	0.34	0.26	0.33

(iii) The powerlike potential introduced in [94],

$$V_{\mathrm{pow}}(r) = a + b r^{\alpha}. \tag{B5}$$

We checked to see that the wave functions obtained with all three potentials have similar shapes. As we mentioned earlier, in the heavy quark mass limit we expect the wave function to be approximated by its behavior near the $r \approx 0$. The wave functions of the P-wave quarkonia have a node at $r \approx 0$, so the relevant parameter, which determines the cross sections in this limit, is the value of the slope $|\mathcal{R}'(0)|^2$. To facilitate comparison with other approaches, in Table II we provide the values of the latter parameter.

For the evaluation of the overlap with gluon wave function (B1), it is convenient to rewrite the quarkonium wave functions in a helicity basis. Conventionally, this is done applying the Melosh-Wigner spin rotation operators defined in [133,134].

[1] G. T. Bodwin, E. Braaten, and G. P. Lepage, Phys. Rev. D **51**, 1125 (1995); **55**, 5853(E) (1997).
[2] F. Maltoni, M. L. Mangano, and A. Petrelli, Nucl. Phys. **B519**, 361 (1998).
[3] N. Brambilla, A. Vairo, and E. Mereghetti, Phys. Rev. D **79**, 074002 (2009); **83**, 079904(E) (2011).
[4] N. Brambilla *et al.*, Eur. Phys. J. C **71**, 1534 (2011).
[5] Y. Feng, J. P. Lansberg, and J. X. Wang, Eur. Phys. J. C **75**, 313 (2015).
[6] S. P. Baranov, A. V. Lipatov, and N. P. Zotov, Eur. Phys. J. C **75**, 455 (2015).
[7] S. P. Baranov and A. V. Lipatov, Phys. Rev. D **96**, 034019 (2017).
[8] J. Adam *et al.* (ALICE Collaboration), J. High Energy Phys. 09 (2015) 148.
[9] B. Trzeciak (STAR Collaboration), J. Phys. Conf. Ser. **668**, 012093 (2016).
[10] R. Ma (STAR Collaboration), Nucl. Part. Phys. Proc. **276–278**, 261 (2016).
[11] D. Thakur (ALICE Collaboration), Springer Proc. Phys. **234**, 217 (2019).
[12] A. Khatun (ALICE Collaboration), Springer Proc. Phys. **261**, 599 (2021).
[13] B. Abelev *et al.* (ALICE Collaboration), Phys. Lett. B **712**, 165 (2012).
[14] B. Abelev *et al.* (ALICE Collaboration), Phys. Lett. B **728**, 25 (2014).
[15] J. Adam *et al.* (ALICE Collaboration), Phys. Lett. B **758**, 389 (2016).
[16] J. Adam *et al.* (ALICE Collaboration), Nat. Phys. **13**, 535 (2017).
[17] D. Thakur (ALICE Collaboration), Springer Proc. Phys. **234**, 217 (2019).
[18] N. Fischer and T. Sjöstrand, J. High Energy Phys. 01 (2017) 140.
[19] V. A. Abramovsky, V. N. Gribov, and O. V. Kancheli, Yad. Fiz. **18**, 595 (1973), https://sciencejournals.ru/journal/yadfiz/.
[20] A. Capella and A. Kaidalov, Nucl. Phys. **B111**, 477 (1976).
[21] L. Bertocchi and D. Treleani, J. Phys. G **3**, 147 (1977).
[22] Y. M. Shabelski, Sov. J. Nucl. Phys. **26**, 573 (1977).

[23] N. N. Nikolaev and W. Schafer, Phys. Rev. D **74**, 074021 (2006).
[24] A. B. Kaidalov and K. A. Ter-Martirosian, Phys. Lett. **117B**, 247 (1982).
[25] E. Levin and M. Siddikov, Eur. Phys. J. C **79**, 376 (2019).
[26] M. Siddikov, E. Levin, and I. Schmidt, Eur. Phys. J. C **80**, 560 (2020).
[27] V. A. Khoze, A. D. Martin, M. G. Ryskin, and W. J. Stirling, Eur. Phys. J. C **39**, 163 (2005).
[28] L. Motyka and M. Sadzikowski, Eur. Phys. J. C **75**, 213 (2015).
[29] E. Gotsman and E. Levin, Eur. Phys. J. C **81**, 99 (2021).
[30] I. Schmidt and M. Siddikov, Phys. Rev. D **101**, 094020 (2020).
[31] M. Siddikov and I. Schmidt, Phys. Rev. D **102**, 076020 (2020).
[32] J. Nielsen *et al.* (ATLAS Collaboration), arXiv:1307.7292.
[33] Apollinari G. *et al.*, CERN Report No. CERN-2017-007-M, 2017, https://cds.cern.ch/record/2284929.
[34] P. La Rocca and F. Riggi, J. Phys. Conf. Ser. **515**, 012012 (2014).
[35] A. K. Likhoded, A. V. Luchinsky, and S. V. Poslavsky, Phys. Rev. D **90**, 074021 (2014).
[36] S. P. Baranov, A. V. Lipatov, and N. P. Zotov, Phys. Rev. D **93**, 094012 (2016).
[37] H. F. Zhang, L. Yu, S. X. Zhang, and L. Jia, Phys. Rev. D **93**, 054033 (2016).
[38] P. Hagler, R. Kirschner, A. Schafer, L. Szymanowski, and O. V. Teryaev, Phys. Rev. Lett. **86**, 1446 (2001).
[39] I. Babiarz, R. Pasechnik, W. Schäfer, and A. Szczurek, J. High Energy Phys. 06 (2020) 101.
[40] A. Cisek and A. Szczurek, Phys. Rev. D **97**, 034035 (2018).
[41] D. Diakonov, M. G. Ryskin, and A. G. Shuvaev, J. High Energy Phys. 02 (2013) 069.
[42] D. Boer and C. Pisano, Phys. Rev. D **86**, 094007 (2012).
[43] L. V. Gribov, E. M. Levin, and M. G. Ryskin, Phys. Rep. **100**, 1 (1983).
[44] L. D. McLerran and R. Venugopalan, Phys. Rev. D **49**, 2233 (1994).
[45] L. D. McLerran and R. Venugopalan, Phys. Rev. D **49**, 3352 (1994).
[46] L. D. McLerran and R. Venugopalan, Phys. Rev. D **50**, 2225 (1994).
[47] A. H. Mueller and J. Qiu, Nucl. Phys. **B268**, 427 (1986).
[48] L. McLerran and R. Venugopalan, Phys. Rev. D **49**, 3352 (1994); **50**, 2225 (1994); **59**, 094002 (1999).
[49] K. J. Golec-Biernat and M. Wusthoff, Phys. Rev. D **60**, 114023 (1999).
[50] B. Z. Kopeliovich and A. V. Tarasov, Nucl. Phys. **A710**, 180 (2002).
[51] B. Kopeliovich, A. Tarasov, and J. Hufner, Nucl. Phys. **A696**, 669 (2001).
[52] Y. V. Kovchegov and E. Levin, *Quantum Chromodynamics at High Energy*, Vol. 33 (Cambridge University Press, Cambridge, England, 2012).
[53] D. Kharzeev and M. Nardi, Phys. Lett. B **507**, 121 (2001); D. Kharzeev and E. Levin, Phys. Lett. B **523**, 79 (2001); D. Kharzeev, E. Levin, and M. Nardi, Phys. Rev. C **71**, 054903 (2005); J. Phys. G **35**, 054001 (2008).
[54] A. Dumitru, D. E. Kharzeev, E. M. Levin, and Y. Nara, Phys. Rev. C **85**, 044920 (2012).
[55] D. Kharzeev and M. Nardi, Phys. Lett. B **507**, 121 (2001).
[56] Y. V. Kovchegov, Nucl. Phys. **A692**, 557 (2001).
[57] E. Levin and A. H. Rezaeian, Phys. Rev. D **82**, 014022 (2010).
[58] T. Lappi, Eur. Phys. J. C **71**, 1699 (2011).
[59] Y. Q. Ma, P. Tribedy, R. Venugopalan, and K. Watanabe, Phys. Rev. D **98**, 074025 (2018).
[60] Y. V. Kovchegov, Phys. Rev. D **61**, 074018 (2000).
[61] V. Barone, M. Genovese, N. N. Nikolaev, E. Predazzi, and B. G. Zakharov, Phys. Lett. B **326**, 161 (1994).
[62] N. N. Nikolaev and B. G. Zakharov, J. Exp. Theor. Phys. **78**, 598 (1994), http://www.jetp.ac.ru/cgi-bin/e/index/e/78/5/p598?a=list.
[63] Y. V. Kovchegov, Phys. Rev. D **60**, 034008 (1999).
[64] Y. V. Kovchegov and H. Weigert, Nucl. Phys. **A784**, 188 (2007).
[65] I. Balitsky and G. A. Chirilli, Phys. Rev. D **77**, 014019 (2008).
[66] Y. V. Kovchegov and E. Levin, Cambridge Monogr. Part. Phys., Nucl. Phys., Cosmol. **33** (2012).
[67] I. Balitsky, Phys. Lett. B **518**, 235 (2001).
[68] F. Cougoulic and Y. V. Kovchegov, Phys. Rev. D **100**, 114020 (2019).
[69] C. A. Aidala *et al.*, arXiv:2002.12333.
[70] Y. Q. Ma and R. Venugopalan, Phys. Rev. Lett. **113**, 192301 (2014).
[71] Y. V. Kovchegov and K. Tuchin, Phys. Rev. D **74**, 054014 (2006).
[72] R. S. Thorne, AIP Conf. Proc. **792**, 324 (2005).
[73] J. Bartels, Nucl. Phys. **B175**, 365 (1980).
[74] J. Kwiecinski and M. Praszalowicz, Phys. Lett. **94B**, 413 (1980).
[75] G. P. Korchemsky, J. Kotanski, and A. N. Manashov, Phys. Rev. Lett. **88**, 122002 (2002).
[76] I. Balitsky, arXiv:hep-ph/9509348; Phys. Rev. D **60**, 014020 (1999); Y. V. Kovchegov, Phys. Rev. D **60**, 034008 (1999).
[77] J. Bartels and E. Levin, Nucl. Phys. **B387**, 617 (1992).
[78] A. M. Stasto, K. J. Golec-Biernat, and J. Kwiecinski, Phys. Rev. Lett. **86**, 596 (2001).
[79] E. Iancu, K. Itakura, and L. McLerran, Nucl. Phys. **A708**, 327 (2002).
[80] E. Levin and K. Tuchin, Nucl. Phys. **B573**, 833 (2000).
[81] E. Iancu, K. Itakura, and S. Munier, Phys. Lett. B **590**, 199 (2004).
[82] H. Kowalski and D. Teaney, Phys. Rev. D **68**, 114005 (2003).
[83] H. Kowalski, L. Motyka, and G. Watt, Phys. Rev. D **74**, 074016 (2006).
[84] G. Watt and H. Kowalski, Phys. Rev. D **78**, 014016 (2008).
[85] A. H. Rezaeian and I. Schmidt, Phys. Rev. D **88**, 074016 (2013).
[86] P. A. Zyla *et al.* (Particle Data Group), Prog. Theor. Exp. Phys. **2020**, 083C01 (2020).
[87] G. Aad *et al.* (ATLAS Collaboration), J. High Energy Phys. 07 (2014) 154.
[88] S. Chatrchyan *et al.* (CMS Collaboration), Eur. Phys. J. C **72**, 2251 (2012).

[89] R. Aaij *et al.* (LHCb), J. High Energy Phys. 10 (2013) 115.
[90] F. Abe *et al.* (CDF Collaboration), Phys. Rev. Lett. **79**, 578 (1997).
[91] A. Abulencia *et al.* (CDF Collaboration), Phys. Rev. Lett. **98**, 232001 (2007).
[92] E. Eichten, K. Gottfried, T. Kinoshita, K. D. Lane, and T. M. Yan, Phys. Rev. D **17**, 3090 (1978); **21**, 313(E) (1980).
[93] E. Eichten, K. Gottfried, T. Kinoshita, K. D. Lane, and T. M. Yan, Phys. Rev. D **21**, 203 (1980).
[94] A. Martin, Phys. Lett. **93B**, 338 (1980).
[95] C. Quigg and J. L. Rosner, Phys. Lett. **71B**, 153 (1977).
[96] J. Bartels and M. G. Ryskin, Z. Phys. C **76**, 241 (1997).
[97] J. Bartels, M. Salvadore, and G. P. Vacca, Eur. Phys. J. C **42**, 53 (2005).
[98] T. Sjostrand and P. Z. Skands, J. High Energy Phys. 03 (2004) 053.
[99] B. Abelev *et al.* (ALICE Collaboration), Phys. Lett. B **712**, 165 (2012).
[100] Y. L. Dokshitzer, V. A. Khoze, and S. I. Troian, J. Phys. G **17**, 1585 (1991).
[101] V. A. Khoze, W. Ochs, and J. Wosiek, arXiv:hep-ph/0009298.
[102] V. A. Khoze and W. Ochs, Int. J. Mod. Phys. A **12**, 2949 (1997).
[103] J. Rafelski and B. Muller, Phys. Rev. Lett. **48**, 1066 (1982); **56**, 2334(E) (1986).
[104] J. Rafelski, Phys. Rep. **88**, 331 (1982).
[105] P. Koch, B. Muller, and J. Rafelski, Phys. Rep. **142**, 167 (1986).
[106] J. Letessier, A. Tounsi, U. W. Heinz, J. Sollfrank, and J. Rafelski, Phys. Rev. Lett. **70**, 3530 (1993).
[107] J. Letessier, J. Rafelski, and A. Tounsi, Phys. Lett. B **328**, 499 (1994).
[108] J. Rafelski and M. Danos, Phys. Rev. C **50**, 1684 (1994).
[109] J. Sollfrank, M. Gazdzicki, U. Heinz, and J. Rafelski, Z. Phys. C **61**, 659 (1994).
[110] J. Letessier, A. Tounsi, U. Heinz, J. Sollfrank, and J. Rafelski, Phys. Rev. D **51**, 3408 (1995).
[111] P. Braun-Munzinger, J. Stachel, J. P. Wessels, and N. Xu, Phys. Lett. B **344**, 43 (1995).
[112] J. W. Harris and B. Muller, Annu. Rev. Nucl. Part. Sci. **46**, 71 (1996).
[113] P. Koch, B. Muller, and J. Rafelski, Int. J. Mod. Phys. A **32**, 1730024 (2017).
[114] J. Rafelski and B. Muller, Phys. Rev. Lett. **48**, 1066 (1982); **56**, 2334(E) (1986).
[115] J. Rafelski, Eur. Phys. J. Special Topics **229**, 1 (2020).
[116] B. Z. Kopeliovich, I. Schmidt, and M. Siddikov, Phys. Rev. C **95**, 065203 (2017).
[117] I. Schmidt, M. Siddikov, and M. Musakhanov, Phys. Rev. C **98**, 025207 (2018).
[118] E. G. Ferreiro and C. Pajares, Phys. Rev. C **86**, 034903 (2012).
[119] B. Z. Kopeliovich, H. J. Pirner, I. K. Potashnikova, K. Reygers, and I. Schmidt, Phys. Rev. D **88**, 116002 (2013).
[120] E. Iancu and A. H. Mueller, Nucl. Phys. **A730**, 460 (2004).
[121] In the literature definitions of the nonintegrated PDF $\mathcal{F}(x, k_\perp)$ might differ by a factor of $k_\perp^2$.
[122] H. G. Dosch, T. Gousset, G. Kulzinger, and H. J. Pirner, Phys. Rev. D **55**, 2602 (1997).
[123] J. D. Bjorken, J. B. Kogut, and D. E. Soper, Phys. Rev. D **3**, 1382 (1971).
[124] S. J. Brodsky, T. Huang, and G. P. Lepage, in *Particles and Fields 2*, edited by A. Z. Capri and A. N. Kamal (Plenum, New York, 1983).
[125] M. V. Terentev, Sov. J. Nucl. Phys. **24**, 106 (1976), https://inspirehep.net/literature/109844.
[126] A. Stadler, S. Leitão, M. T. Peña, and E. P. Biernat, Few-Body Syst. **59**, 32 (2018).
[127] D. Daniel, R. Gupta, and D. G. Richards, Phys. Rev. D **43**, 3715 (1991).
[128] T. Kawanai and S. Sasaki, Phys. Rev. Lett. **107**, 091601 (2011).
[129] T. Kawanai and S. Sasaki, Phys. Rev. D **89**, 054507 (2014).
[130] J. Nemchik, N. N. Nikolaev, E. Predazzi, and B. G. Zakharov, Z. Phys. C **75**, 71 (1997).
[131] J. Hufner, Y. P. Ivanov, B. Z. Kopeliovich, and A. V. Tarasov, Phys. Rev. D **62**, 094022 (2000).
[132] Technically, we expect that the spin-angular dependence will contribute via overlap with the helicity-dependent wave function of the gluon [Eq. (B1)].
[133] H. J. Melosh, Phys. Rev. D **9**, 1095 (1974).
[134] W. Jaus, Phys. Rev. D **41**, 3394 (1990).